第35卷第6期
2016年12月

红外与毫米波学报
J. Infrared Millim. Waves

Vol. 35, No. 6
December, 2016

文章编号: 1001-9014(2016)06-0646-06

DOI: 10.11972/j.issn.1001-9014.2016.06.002

Hybrid functional calculation of electronic structure of InAs/GaSb superlattice in (111) orientation

YAO Lu-Chi [1,2], ZHOU Xiao-Hao [1], CHEN Xiao-Shuang [1*]

(1. National Key Laboratory of Infrared Physics, Shanghai Institute of Technical Physics, Chinese Academy of Sciences, Shanghai 200083, China;
2. University of Chinese Academy of Sciences, Beijing 100049, China)

Abstract: Electronic structures and band structures of a series of InAs/GaSb superlattice in (111) orientation were calculated by density functional theory (DFT) method. Heyd-Scuseria-Ernzerhof (HSE) hybridization coupled with revised Perdew-Burke-Ernzerhof (PBE) approximation for solids and surfaces (PBEsol) showed better consistency with the experimental measurements than conventional DFT and several compared hybrid functionals. The bandgap changes with periodic thickness and InAs/GaSb ratio of InAs/GaSb superlattice. The results are in good agreement with the former experimental researches. These results indicate the feasibility of HSE coupled with PBEsol method in prediction of the electronic properties of InAs/GaSb superlattice.

Key words: first-principles method, hybrid functional, InAs/GaSb type-II superlattice, band structure calculation
PACS: 73.21.-b, 85.30.De

(111)方向的InAs/GaSb超晶格材料电子结构的杂化泛函计算

姚路驰[1,2]， 周孝好[1]， 陈效双[1*]

(1. 中国科学院上海技术物理研究所 红外物理国家重点实验室,上海 200083;
2. 中国科学院大学,北京 100049)

摘要:采用电子密度泛函理论方法计算了一系列(111)方向的InAs/GaSb超晶格的电子结构和能带结构.将杂化泛函的计算结果与普通密度泛函方法的计算结果进行了比较. Heyd-Scuseria-Ernzerhof (HSE)杂化与对固体修正的Perdew-Burke-Ernzerhof (PBE)近似结合的杂化泛函显示了较传统PBE方法和若干其他杂化泛函更符合实验数据的结果.采用该方法研究了InAs/GaSb超晶格的带隙随超晶格周期厚度以及InAs/GaSb比例变化的规律.其结果与以往实验结果符合很好.这些结果表明HSE-PBEsol方法对于估计InAs/GaSb超晶格的电子性质适用.

关　键　词:第一性原理方法;杂化泛函;II类超晶格;能带计算

中图分类号:TN213　　**文献标识码**:A

Introduction

InAs/GaSb type-II superlattice structure has attracted extensive research interests after it was proposed by Esaki *et. al*[1]. Because the conduction band bottom of InAs bulk is lower than the valence band top of GaSb bulk, the bandgap of short-period InAs/GaSb type-II superlattice is determined by interfacial state and piezoelectric polarization and can be continuously modulated by thickness, composition and strain of InAs/GaSb layers. Significant advantages, such as thinckness-dependent bandgap, broad spectral response range (3 ~ 30 μm) and low tunneling current make InAs/GaSb superlattice be a promising candidate for the third generation photon detectors[2]. In recent years, InAs/GaSb superlattice de-

Received date: 2016-03-01, **revised date**: 2016-09-28　　**收稿日期**:2016-03-01, **修回日期**:2016-09-28

Foundation items: Supported by State Key Program for Basic Research of China (2013CB632705, 2011CB922004), National Natural Science Foundation of China (11334008, 61290301), Fund of Shanghai Science and Technology Foundation (13JC1408800)

Biography: YAO Lu-Chi (1989-), male, Yangzhou, China. Ph. D. Research interests focus on electronics and optoelectronics of Si and III-V materials based on first-principles methods. E-mail: lcyao@mail.sitp.ac.cn

* **Corresponding author**: E-mail: xschen@mail.sitp.ac.cn

vices have been rapidly developed. Single-element detector[3], focal plane arrays[4], dual-color arrays[5], have been fabricated. Though most InAs/GaSb supperlattice were epitaxially grown along (100) or (110) direction, the InAs/GaSb supperlattice grown along (111) direction with abrupt InAs/GaSb interface was found to perform better[6].

The broadening applications and increasingly complex synthesis process of InAs/GaSb devices urge deep and detailed understanding of the electronic properties of InAs/GaSb superlattice structure. Several theoretical methods have been applied to investigate the electronic properties of superlattice structures, such as envelope-function approximation (EFA)[7], empirical tight-binding method (ETBM)[8] and density functional theory (DFT)[9]. Among these methods, DFT methods get universal application and recognition because DFT methods are independent of any empirical or experimental parameters to predict material properties. In addition, it is more convenient to take strain, doping into consideration by applying DFT method.

However, the conventional DFT methods, such as local-density approximation (LDA) and generalized gradient approximation (GGA), systematically underestimate the bandgaps of semiconductors, especially when $3d$ orbitals exist. For example, the bandgaps of InAs and GaSb are predicted to be 0 by GGA methods. This failure of bandgap prediction is ascribed to the approximation of quasi-particle in average potential field and the strong correlation effects between $3d$ electrons. To correct these errors, a hybrid functional approach was built by hybridizing the conventional DFT functionals with the exact Hartree-Fock exchange functional[10-12].

In this work, we provide the electronic structure and band structure of InAs/GaSb type-II superlattice of various thickness in (111) orientation by hybrid functional DFT calculations. These results were compared with former experimental and theoretical researches.

1 Methods

Standard periodic $(InAs)_m/(GaSb)_n$ models in (111) orientation of zinc blende structure with abrupt InAs/GaSb interfaces was built, as shown in Fig. 1. m (n) = 1, 2, 3, 6, 9, 12 is the number of molecule layers (MLs) of InAs (GaSb). InAs/GaSb superlattice structures with different period and InAs/GaSb ratio were investigated by combined different m with n. In this way, the variations of electric and band structure with the period and InAs(GaSb) thicknesses were provided. Because of the symmetry of (111) direction, the period of the models should be integer multiples of 3. So in cases where $m+n$ is indivisible by 3, models of three period $(InAs)_m/(GaSb)_n$ structures were built. Because of the ultra-expensive computational consumption, only models of less than 18 MLs were processed.

Several alternative hybrid functionals can be used to calculate electronic structures, such as B3LYP (Becke, three-parameter, Lee-Yang-Parr)[10], PBE0[11], and HSE06 (Heyd-Scuseria-Ernzerhof)[12]. B3LYP functional is universally applicable to most of materials and can provide acceptable results. PBE0 and HSE06mix

Fig. 1 Schematic diageram of $(InAs)_m/(GaSb)_n$ superlattice along (111) direction
图 1 沿(111)方向的$(InAs)_m/(GaSb)_n$超晶格结构示意图

Hartree-Fock exchange energy with the PBE (Perdew-Burke-Ernzerhof)[13] exchange energy. HSE functional can be regarded as a high-efficiency version of PBE0. So we tested the accuracy of B3LYP and HSE06 functional in prediction of InAs and GaSb band structure and compared the results with the results from experiments and conventional PBE calculations. In addition, PBEsol[14], a revised version of PBE functional for solids, was also calculated coupled with HSE06 hybrid functional.

All the DFT calculations are performed by the VIENNA AB INITIO SIMULATION PACKAGE (VASP)[15-16]. The electron - ion interaction was described by the projector-augmented-wave (PAW)[17] method with a plane-wave energy cutoff of 400 eV. The Gaussian smearing method was applied to determine the electronic occupation and the width of smearing was set as 0.1 eV. The Brillouin zones of the models are sampled by the Monkhorst - Pack grids of k-point. The k-point mesh of $7\times7\times7$ and $5\times5\times1$ is found accurate enough to InAs/GaSb unit cell and superlattice structure calculations, respectively. All models have been fully relaxed by corresponding potentials before static calculation. In the relaxation calculations of these structures, the convergence in energy and force is set as 10^{-5} eV and 10^{-3} eV/Å, respectively.

2 Results and discussions

2.1 DFT methods comparison and hybrid functional selection

The bandgap results of solid InAs and GaSb by the above methods (PBE, HSE-PBE, HSE-PBEsol and B3LYP) are shown in Table 1. And the band structure results of solid InAs and GaSb by HSE06 coupled with PBEsol (HSE-PBEsol) and conventional PBE are shown in Fig. 2. As mentioned above, the conventional PBE method failed to predict the bandgap of both InAs and GaSb. Benefiting from the introduction of the exact exchange energy, all three hybrid functionals present the narrow bandgap of both InAs and GaSb crystals. Compared with HSE-PBE and B3LYP methods, HSE-PBEsol method performs well for both solid InAs and GaSb. So we applied HSE-PBEsol method in calculations of InAs/GaSb superlattice structures.

2.2 Influence of periodic thickness on electronic structure of InAs/GaSb superlattice

Periodic thickness is a key parameter in device design and engineering of InAs/GaSb superlattice detectors. The periodic thickness of InAs/GaSb superlattice has highly important influences on response range, abs-

Table 1 Comparison of the calculated bandgaps of solid InAs and GaSb by several DFT methods and the experimental results (experimental results are collected from Ref. [18])

表1 不同电子密度泛函方法所得 InAs 和 GaSb 晶体禁带宽度与实验值对比(实验数据摘自文献[18])

Material	Bandgap E_g/eV				
	Exp. [18]	PBE	HSE-PBE	HSE-PBEsol	B3LYP
InAs	0.42	0.00	0.36	0.45	0.43
GaSb	0.81	0.00	1.02	0.99	0.34

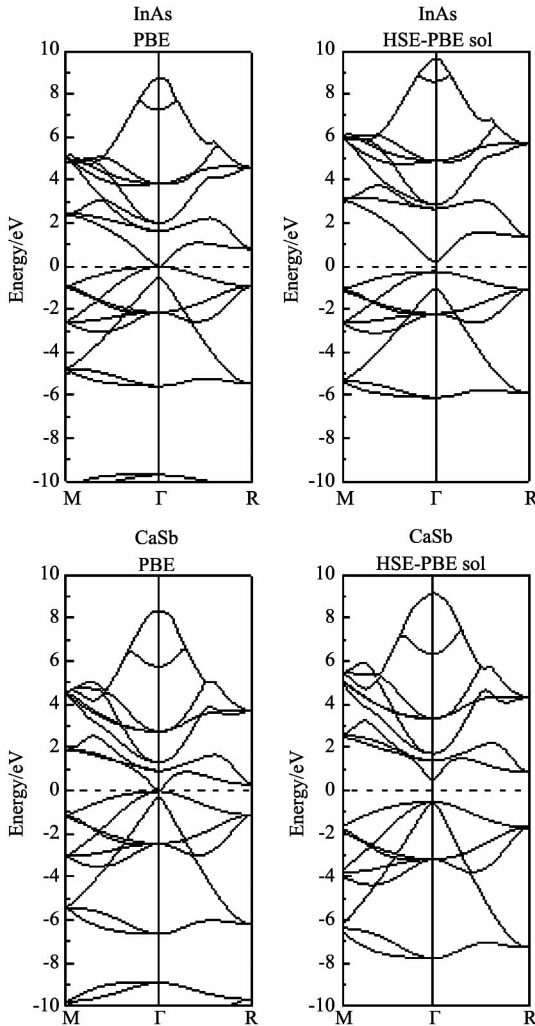

Fig. 2 Band structures of solid InAs and GaSb calculated by PBE and HSE-PBEsol methods (the calculated fermi energy of InAs and GaSb are 2.93 eV and 3.68 eV, respectively, in a comparison sense)

图2 PBE 和 HSE-PBEsol 方法计算所得 InAs 和 GaSb 晶体的能带结构(计算中 InAs 和 GaSb 的费米能级分别为2.93 eV、3.68 eV,该值仅具有相对比较意义)

orption coefficient and dimension of the device. We calculated a series of $(InAs)_n/(GaSb)_n$ superlattice structures ($n=1, 2, 3, 6, 9$) to investigate the influence of periodic thickness on the electronic structure of InAs/GaSb. The structures with the same thickness of InAs and GaSb ML(s) were applied to directly reveal the influence of periodic thickness.

The bandgap changes with the periodic thickness of the $(InAs)_n/(GaSb)_n$ superlattice structures ($n=1, 2, 3, 6, 9$) are shown in Fig. 3. The gradual decrease of the bandgap with periodic thickness increase when $n>3$ conforms to former investigations[19]. Moreover, the cut-off wave length of $(InAs)_6/(GaSb)_6$ and $(InAs)_9/(GaSb)_9$ is 4.33 μm and of 4.83 μm, respectively. The results is in good consistency of the former reported measurement of cut-off wave length of $(InAs)_7/(GaSb)_7$ superlattice (4.2 μm)[5] and of $(InAs)_{10}/(GaSb)_{10}$ superlattice (5.6 μm)[12]. These results indicate the robust performance of HSE-PBEsol method in InAs/GaSb superlattice systems. As a rough estimation, we can extrapolate the bandgap would vanish when the periodic thickness increases to over 160Å.

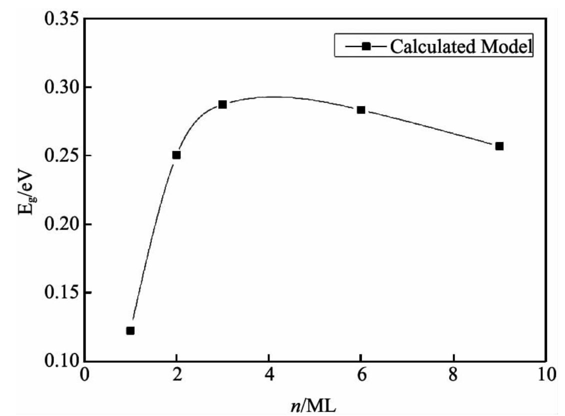

Fig. 3 Bandgap changes with the periodic thickness of the $(InAs)_n/(GaSb)_n$ superlattice structures. ($n=1, 2, 3, 6, 9$)

图3 带隙随$(InAs)_n/(GaSb)_n$超晶格结构周期厚度变化图($n=1, 2, 3, 6, 9$)

The sharp decrease of the bandgap with periodic thickness decrease when $n<3$ is counter-intuitive. However, in view of that $(InAs)_1/(GaSb)_1$ is very similar to $(GaAs)_1/(InSb)_1$ (the two symbols are identical in (100) direction and slightly different in bonding in (111) direction), the perfect $(GaAs)_1/(InSb)_1$ structure should display a bandgap smaller than InSb (0.24 eV). This effect will rapidly be neutralized by the increase of periodic thickness. This argument can be supported by distribution change of the valence band maximum (VBM) and conduction band minimum (CBM) with the periodic thickness. As shown in Fig. 4, when $n>3$, the $(InAs)_n/(GaSb)_n$ supperlattices are typical type-II superlattices with significant electron-hole separation. However, when $n<3$, the increase of electron density at the In-Sb interface and the increase of hole density at the Ga-As interface can be observed. It means that these superlattices with ultra-short period are not typical type-II superlattices but some polarization dominated systems.

We supposed that the polarization in InAs/GaSb superlattice also narrows the band gap. Because of the asymmetric polarized (111) surfaces and the 0.7% mis-

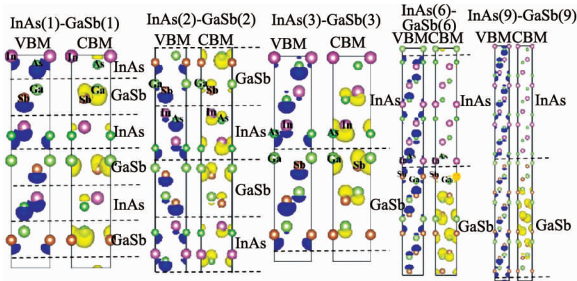

Fig. 4 The VBM and CBM of a series of $(InAs)_n/(GaSb)_n$ superlattice structures. The blue regions represent the VBM, and the yellow regions represent the CBM. The pink, smaller green, larger green and brown balls represent In, As, Ga and Sb atoms, respectively. (n = 1, 2, 3, 6, 9)

图 4 一系列$(InAs)_n/(GaSb)_n$超晶格结构的价带顶与导带底的分布图. 其中蓝色区域代表价带顶,黄色区域代表导带底,粉色、较小绿色、较大绿色和棕色小球分别表示 In、As、Ga、Sb 原子. (n = 1, 2, 3, 6, 9)

match of InAs and GaSb, spontaneous polarization and piezoelectric polarization both exist in the $(InAs)_m/(GaSb)_n$ structures along (111) direction. The difference charge densities of a series of $(InAs)_n/(GaSb)_n$ superlattice structures (n = 1, 2, 3, 6, 9) compared with pure InAs or GaSb structures of the same size were present in Fig. 5 to show the polarization. Electrons transfer from the Ga-As bond to the In-Sb bond. So the electrons at the In-Sb bond occupy high states and narrow the bandgaps of these superlattices. And no significant distribution changes of the difference charge densities with period variation were observed. Because that piezoelectric polarization is linear to film thickness (if film is not broken), we supposed the electron transition is caused by spontaneous polarization. So influence of the intrinsic polarization should recede with the periodic thickness increase.

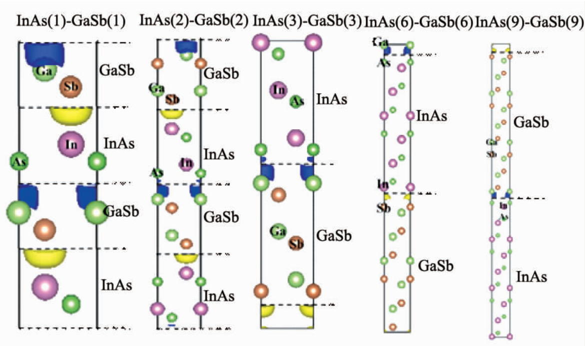

Fig. 5 The difference charge densities of a series of $(InAs)_n/(GaSb)_n$ superlattice structures. The yellow regions represent the increase of charge densities, and the blue regions represent the decrease of charge densities. The pink, smaller green, larger green and brown balls represent In, As, Ga and Sb atoms, respectively. (n = 1, 2, 3, 6, 9)

图 5 一系列$(InAs)_n/(GaSb)_n$超晶格结构的差分电荷密度图. 其中黄色区域代表电荷增加,蓝色区域代表电荷减少,粉色、较小绿色、较大绿色和棕色小球分别表示 In、As、Ga、Sb 原子. (n = 1, 2, 3, 6, 9)

2.3 Influence of InAs/GaSb ratio on the bandgap of InAs/GaSb superlattice

Besides the thickness, the InAs/GaSb ratio of the InAs/GaSb superlattice, i. e. the asymmetric thickness of InAs and GaSb layers is also a key parameter in detector design. The response range can be precisely tuned by adjusting InAs/GaSb ratio, especially in dual-color or multi-color detectors in which superlattice thicknesses should be carefully designed. We calculated the bandgap of a series of $(InAs)_m/(GaSb)_n$ superlattice structures to investigate the bandgap change with the InAs or GaSb thickness. Because of the compute capability limit, we limited m, n to be multiples of three, and $m + n < 15$ except $(InAs)_9/(GaSb)_9$. The bandgap values of the models are shown in Table 2.

Table 2 Bandgap values of $(InAs)_m/(GaSb)_n$ superlattice structures

表 2 一系列$(InAs)_m/(GaSb)_n$超晶格结构的带隙

E_g/eV		m/ML			
		3	6	9	12
n/ML	3	0.287	0.188	0.158	0.131
	6	0.304	0.283	0.239	-
	9	0.319	0.298	0.257	-
	12	0.334	-	-	-

Figure 6 shows the changes of bandgap and cut-off wavelength of $(InAs)_m/(GaSb)_n$ superlattice structures with different thicknesses of GaSb. The thickness of InAs was fixed to be 3/6/9 MLs. Broadening of band gap and blue shift of cut-off wavelength with increase of the thickness of GaSb can be observed. This observation is similar to former experimental and theoretic researches. So reducing the GaSb layer thickness is a possible way to adjust the response range of InAs/GaSb superlattice devices.

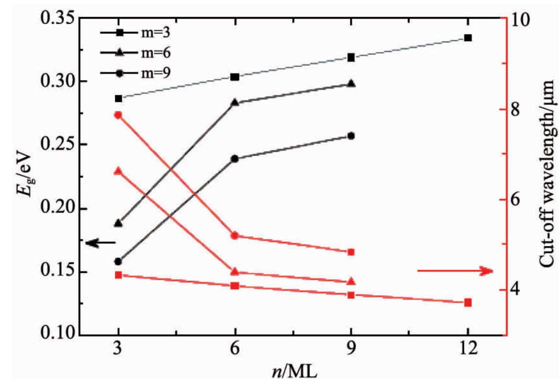

Fig. 6 Bandgap and cut-off wavelength changes of $(InAs)_m/(GaSb)_n$ superlattice structures with different thicknesses of GaSb

图 6 带隙和截止波长随$(InAs)_m/(GaSb)_n$超晶格结构中 GaSb 层厚度变化图

Figure 7 reveals the changes of bandgap and cut-off wavelength of $(InAs)_m/(GaSb)_n$ superlattice structures with different thicknesses of InAs. The thickness of GaAs was fixed to be 3/6/9 MLs. Narrowing of the bandgap

and red shift of cut-off wavelength with increase of thickness of InAs can be observed. Noted that the changes of bandgap and response wavelength with the thickness of InAs are much more sharp than the changes with the thickness of GaSb. It means that increasing the thickness of InAs is a more efficient approach to increase the cut-off wave length. In addition, the cut-off wavelength of $(InAs)_9/(GaSb)_9$ (4.83 μm) is in good consistency with the experimental measurement of the cut-off wavelength of $(InAs)_9/(GaSb)_{12}$ (4.6 μm)[19]. Taking the blue shift caused by the increased thickness of GaSb into consideration, we suppose the HSE-PBEsol method combined with standard InAs/GaSb models shows very present reliable predicition of bandgap properties of InAs/GaSb superlattice systems.

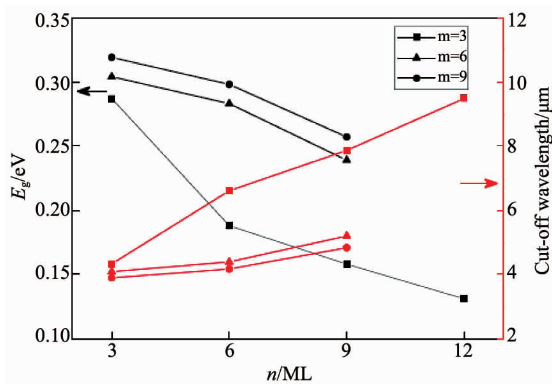

Fig. 7 Bandgap and cut-off wavelength changes of $(InAs)_m/(GaSb)_n$ superlattice structures with different thicknesses of InAs

图 7 带隙和截止波长随$(InAs)_m/(GaSb)_n$超晶格结构中 InAs 层厚度变化图

In direct-gap semiconductors, absorption coefficient is inversely proportional to the film thickness. So achieving the target cut-off wavelength in minimum periodic thickness is an important design principle of InAs/GaSb superlattice detectors. The cut-off wavelength can be adjusted by changing the InAs/GaSb ratio in InAs/GaSb superlattice of a certain periodic thickness. The variations of bandgap and cut-off wavelength of InAs/GaSb superlattice with equal periodic thickness while different thicknesses of InAs are shown in Fig. 8. A series of InAs/GaSb superlattice of 12/15 ML thick with InAs thickness changing from 3 ML to 12 ML were present. The results indicate that the range of cut-off wavelength from 4μm to10μm can be achieved in InAs/GaSb superlattice of 15 ML thick.

3 Conclusion

Electronic structures and band structures of a series of InAs/GaSb superlattice were calculated by DFT method. Hybrid functional methods were applied in DFT calculations and compared with conventional DFT results. We found that HSE methods coupled with PBEsol exchange-correlation potential shows more consistency with the experimental measurements than conventional PBE, HSE-PBE and B3LYP methods. The bandgap variations

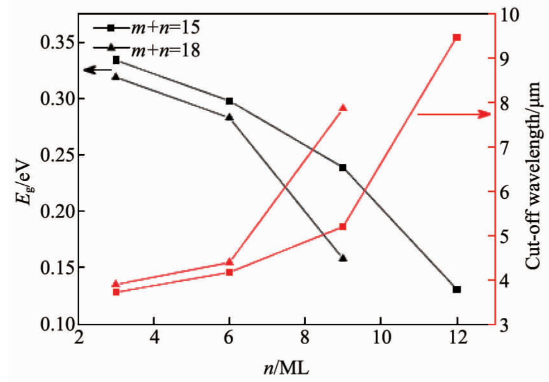

Fig. 8 Bandgap and cut-off wavelength changes of InAs/GaSb superlattice structures with equal periodic thickness and different thicknesses of InAs

图 8 等周期厚度 InAs/GaSb 超晶格结构中带隙和截止波长随 InAs 厚度变化图

with periodic thickness and InAs/GaSb ratio of InAs/GaSb superlattice structures were investigated. The results in good agreement with the former theoretical and experimental researches indicate the feasibility of HSE-PBEsol method to guide the design of InAs/GaSb superlattice devices.

Acknowledgement

This work was supported by the State Key Program for Basic Research of China (2013CB632705, 2011CB922004), the National Natural Science Foundation of China (11334008, 61290301), the Fund of Shanghai Science and Technology Foundation (13JC1408800).

References

[1] Sa-Halasz G A, Tsu R, Esaki L. A new semiconductor superlattice [J]. *Applied Physics Letters*, 1977, **30**(12): 651-653.

[2] Rogalski A. Material consideration for third generation infrared photon detectors [J]. *Infrared Physics and Technology*, 2007, **50**(2-3): 240-252.

[3] Johnson H J, Samoska L A, Gossard A C, *et al*. Electrical and optical properties of infrared photodiodes using the $InAs/Ga_{1-x}In_xSb$ superlattice in heterojuntions with GaSb [J]. *Journal of Applied Physics*, 1996, **80**(2): 1116-1127.

[4] XU Qing-Qing, CHEN Jian-Xin, ZHOU Yi, *et al*. Mid-wavelength infrared InAs/GaSb type II superlattice detectors[J]. *Infrared and Laser Engineering*(徐庆庆, 陈建新, 周易, 等. InAs/GaSb II 类超晶格中波红外探测器, **红外与激光工程**), 2012, **41**(1): 7-9.

[5] BAI Zhi-Zhong, XU Zhi-Cheng, ZHOU Yi, *et al*. 320×256 dual-color mid-wavelength infrared InAs/GaSb superlattice focal plane arrays [J]. *Journal of Infrared and Millimeter Waves*(白治中, 徐志成, 周易, 等. 320×256 元 InAs/GaSb II 类超晶格中波红外双色焦平面探测器, **红外与毫米波学报**), 2012, **34**(6): 716-720.

[6] Plis E, Klein B, Myers S, *et al*. Type-II InAs/GaSb strained layer superlattices grown on GaSb (111)B substrate [J]. *Journal of Vacuum Science & Technology B*, 2013, **31**(3): 03C123.

[7] Bastard G. Theoretical investigations of superlattice bandstructure in the envelope-function approximation [J]. *Physical Reviews B*, 1982, **25**(12): 7584-7597.

[8] Wei Y J, Razeghi M. Modeling of type-II InAs/GaSb superlattices u-

sing an empirical tight-binding method and interface engineering [J]. *Physical Reviews B* 2004, **69**(8): 085316.

[9] Wang J W, Zhang Y. Band-gap corrected density functional theory calculations for InAs/GaSb type II superlattices [J]. *Journal of Applied Physics*, 2014, **116**(21): 214301.

[10] Stephens P J, Devlin F J, Chabalowski C F, *et al*. Ab initio calculation of vibrational absorption and circular dichroism spectra using density functional force fields [J]. *The Journal of Physical Chemisty*, 1994, **98**(45): 11623-11627.

[11] Adamo C, Barone V. Toward reliable density functional methods without adjustable parameters: The PBE0 model [J]. *The Journal of Chemical Physics*, 1999, **110**(13): 6158-6170.

[12] Heyd J, Scuseria G E, Ernzerhof M. Hybrid functionals based on a screened Coulomb potential [J]. *The Journal of Chemical Physics*, 2003, **118**(18): 8207.

[13] Perdew J P, Burke K, Ernzerhof M. Generalized gradient approximation made simple [J]. *Physical Review Letters*, 1996, **77**(18): 3865.

[14] Perdew J P, Ruzsinszky A, Csonka G I, *et al*. Restoring the density-gradient expansion for exchange in solids and surfaces [J]. *Physical Review Letters*, 2009, **100**(13): 136406.

[15] Kresse G, Furthmüller J. Efficiency of ab-initio total energy calculations for metals and semiconductors using a plane-wave basis set [J]. *Computational Materials Science*, 1996, **6**(1): 15.

[16] Kresse G, Furthmüller J. Efficient iterative schemes for ab initio total-energy calculations using a plane-wave basis set [J]. *Physical Review B*, 1996, **54**(16): 11169.

[17] Blöchl P E. Projector augmented-wave method [J]. *Physical Review B*, 1994, **50**: 17953.

[18] Hinuma Y, Grüneis A, Kresse G, *et al*. Band alignment of semiconductors from density-functional theoryand many-body perturbation theory [J]. *Physical Review B*, 2014, **90**: 155405.

[19] ZHOU Yi, CHEN Jian-Xin, HE Li. Band structure calculation of InAs/GaSb superlattice under 4 layers model [J]. *Journal of Infrared and Millimeter Waves* (周易, 陈建新,何力. 四层结构模型下的InAs/GaSb 超晶格材料能带计算, **红外与毫米波学报**), 2013, **32**(1): 13-17.